Polypeptide Adsorption on a Synthetic Montmorillonite: A Combined Solid-State NMR Spectroscopy, X-ray Diffraction, Thermal Analysis and N_2 Adsorption Study

Régis D. Gougeon,*[a] Michel Soulard,[b] Marc Reinholdt,[b] Jocelyne Miehé-Brendlé,[b] Jean-Michel Chézeau,[b] Ronan Le Dred,[b] Richard Marchal,[a] and Philippe Jeandet*[a]

Keywords: Peptides / Adsorption / Clays / NMR spectroscopy / X-ray diffraction

Two homopolypeptides, polylysine and polyglutamic acid, were adsorbed on a synthetic montmorillonite clay, in acidic medium. These organic-inorganic complexes can be heated up to 110 °C without any degradation of the polypeptide. ^{1}H-^{13}C CP-MAS NMR spectra show that these polypeptides, which exhibit a mixture of α-helical and random coil conformations in the bulk, tend to unfold and adopt a more extended random coil structure on adsorption on the phyllosilicate. The values of the basal spacing measured by X-ray diffraction on dehydrated samples clearly indicate that in the presence of adsorbed polypeptide, the silicate layers do not collapse. The incorporation of polypeptide fragments within the interlayer space is also revealed by the decrease in the specific surface areas measured by N_2-adsorption BET experiments.

Introduction

Specific interactions between polymers or proteins and clay mineral solid surfaces are at the basis of both natural processes and technological applications. In soil chemistry for instance, such organic-inorganic interactions are considered to be of prime importance in the regulation of the microbially mediated decomposition processes of soil organic matter.[1] Alternatively, membrane filtration[2] or advanced hybrid materials[3,4] are examples of the efficient use of the macromolecule-clay mineral interactions for new industrially relevant techniques. On the other hand, bentonites have been used for more than 60 years as adsorbents in winemaking, to remove proteins from musts and wines.[5] This particular affinity of proteins for phyllosilicates is based on the commonly high specific-surface areas associated with swelling and cation-exchange properties of the latter. Due to intralayer octahedral and/or tetrahedral substitutions, montmorillonites exhibit an overall negative surface charge that is balanced by hydrated cations such as sodium or calcium which are located within the interlayer spaces.[6] At pH values below their isoelectric points (i.e.p.), proteins are positively charged and their adsorption is basically seen as a cation-exchange process based on electrostatic, hydrophobic and/or hydrophilic interactions.[7]

To characterize the way in which proteins interact with solid surfaces, several studies have pointed out the important features arising from the modification of the conformation of interacting macromolecules. In particular, FTIR and enzymatic activity studies have emphasized the pH-dependent modification[8] and/or pH-dependent orientation[9] effects on the adsorbed enzymes, characterized by structural unfolding due to electrostatic interactions with montmorillonite. However, the mechanisms by which proteins are adsorbed on clay minerals are still subject to many questions.[10] A detailed description of the part of the protein that interacts with the mineral surface and the distance of interaction is required to understand the proteins/solid surface interactions.[11]

The aim of this study is to investigate model samples that can be considered as representative of protein−clay mineral complexes. This is accomplished through the analysis of the adsorption of two homopolypeptides, polylysine and polyglutamic acid (Scheme 1), on a synthetic montmorillonite,[12] using complementary approaches.

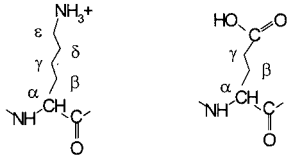

Scheme 1. Lysine (left) and glutamic acid (right) units

[a] Laboratoire d'œnologie URVVC, Université de Reims, UPRES EA 2069, Faculté des Sciences,
Moulin de la Housse, B. P. 1039, 51687 Reims Cedex 2, France
[b] Laboratoire de Matériaux Minéraux, Ecole Nationale Supérieure de Chimie, UMR-CNRS 7016,
3, Rue A. Werner, 68093 Mulhouse cedex, France

Thermal analyses (TG-DTA) can provide a rather accurate determination of the amount of adsorbed polypeptides on the solid surfaces,[13] and can also afford useful indirect information about the strength of the organic-inorganic interaction, from the decomposition temperature of the organic matter.[14]

Despite its low sensitivity, solid-state NMR spectroscopy has been successfully applied to the study of interfaces. In particular, this technique does not require any mechanical treatment and can provide, under certain circumstances, a direct three-dimensional picture of polypeptides in the bulk or in the adsorbed state.[13,15] Solid-state NMR spectroscopy has already been applied to the qualitative and/or quantitative characterization of soil organic matter,[16] but rarely to the characterization of adsorbed proteins on clay minerals.[17]

Several features can be obtained from powder X-ray diffraction patterns of smectites, e.g. the basal spacing, which is equal to the sum of the interlayer spacing and the thickness of the silicate layer, and which is given by the measurement of the (001) peak position.[18] Numerous studies have reported the d_{001} values of clay minerals onto which organic molecules such as amino acids[19] or alkylammonium ions[20] were adsorbed. These results provide a good basis for the comparison of values measured for polypeptide-adsorbed montmorillonite, either under controlled humidity or after dehydration.

Finally, one of the most interesting properties to explore when dealing with porous solids is the specific surface area and its variation resulting from the adsorption of organic molecules. However, measuring the actual specific surface area of montmorillonites corresponds to the determination of the surface area between the silicate layers which, in the absence of any adsorbed molecule, is theoretically equal to 760 m^2/g.[21] Such a result is classically obtained by the adsorption of a probe molecule such as methylene blue,[22] which can displace some interlayer species, and therefore cannot be used in the presence of previously adsorbed polypeptides. Consequently, nitrogen was used to determine the BET surface areas. It must be noted that the whole interlayer microporous surface of montmorillonites is theoretically not accessible to nitrogen molecules owing to the reversible collapse of the silicate layers on outgassing.

Results and Discussion

Thermal Analyses

The DTA curve (Figure 1, a) of the synthetic montmorillonite (**M**) is characterized by a major endothermic peak at 100 °C, which corresponds to interlayer dehydration, followed by a second weaker and broader endothermic peak, with a minimum at 650 °C, for the dehydroxylation of the layer.[12] On adsorption of polypeptides, the DTA curves (Figure 1, a) show additional exothermic signals in the range 260−700 °C, which correspond to the oxidative degradation of the adsorbed organic molecules. For **M/PL**, a strong exothermic peak occurs at 320 °C, and is followed by a second weaker exothermic peak at 600 °C. Two broader peaks are also observed for **M/PG**, but with weaker intensities and with the first peak occurring at a higher temperature than that for **M/PL**.

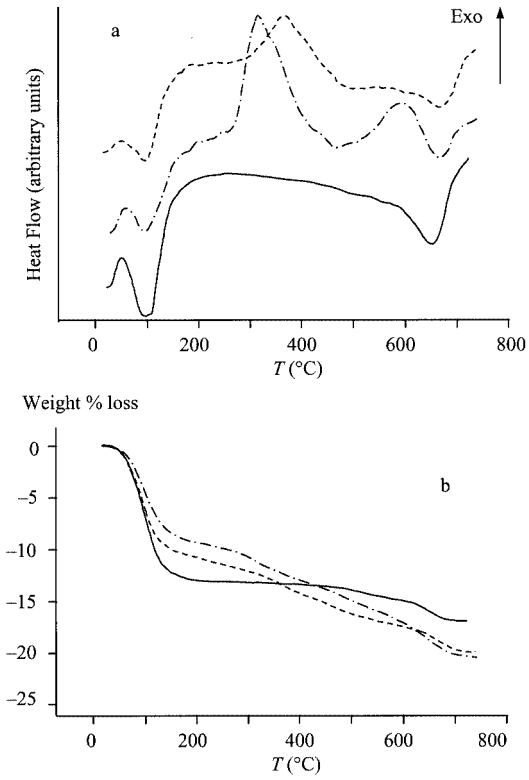

Figure 1. (a) DTA and (b) TG curves of **M** (plain line), **M/PL** (dashed dotted line) and **M/PG** (dotted line)

The amounts of adsorbed polypeptide were determined from the analysis of the TG curves (Figure 1, b), since the distinct exothermic peaks are solely due to the combustion of the organic matter. However, weight losses recorded at higher temperatures include the dehydroxylation process. The latter can be quantified from the experiment on **M** alone, and then subtracted from the weight losses determined for the organic-inorganic complexes. Table 1 gathers the calculated amounts of **PL**, **PG** and **PL/PG** adsorbed on **M**. For each separate adsorption (**M/PL** and **M/PG**), nearly all the polypeptide introduced is adsorbed. When both polypeptides are simultaneously introduced, and in higher quantities (**M/PL/PG**), they are also almost completely adsorbed (Table 1). In the case of **M/PL/PG**, the amount of **PL** introduced was set to present approximately 100 mequiv. of side chain NH_3^+ charges per 100 g of calcined

Table 1. Weight-percent amount, relative to dehydrated montmorillonite, of polypeptide introduced and adsorbed, from TG analyses; errors are ± 0.2

	M/PL	M/PG	M/PL/PG
Introduced	7.0	5.0	12.0 + 12.0
Adsorbed	7.0	4.7	21.0
After outgassing	4.6	3.3	20.3

montmorillonite, i.e. the initial cation exchange capacity of **M**.[12] Therefore, if **PL** is adsorbed via an electrostatic mechanism, in order to replace the Na^+ cations and balance the negative charge of **M**, **PG**, which does not bear positively charged side chains, is adsorbed via a different mechanism.

In order to assess the thermal stability of these organic-inorganic complexes, similar TG-DTA measurements were performed on the samples which had previously been outgassed under vacuum to a temperature of 110 or 150 °C, as required for nitrogen adsorption experiments. The corresponding weight losses are also given in Table 1. On outgassing at 150 °C under vacuum, both **M/PL** and **M/PG** have lost part of the initial amount of adsorbed organic matter. This loss of matter is higher for **M/PL** than for **M/PG**. In contrast, the total amount of adsorbed **PL** and **PG** is kept unchanged after having heated **M/PL/PG** to 110 °C, under vacuum. Furthermore, as shown below by ^{13}C NMR spectroscopy, the structure of the remaining adsorbed polypeptides is kept unchanged, which indicates that outgassing has basically lowered the amount of adsorbed matter, and that any decomposition products, volatile or not, have been outgassed.

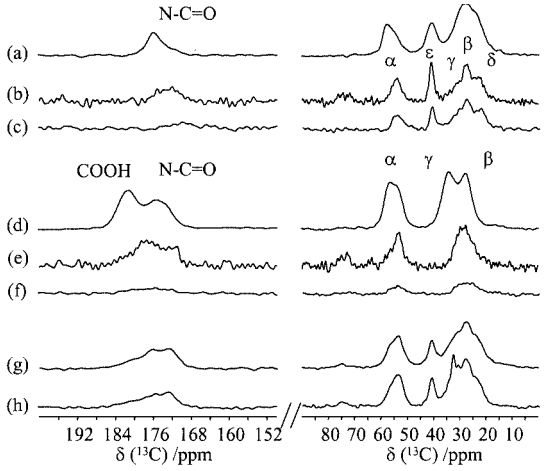

Figure 2. ^1H-^{13}C CP-MAS spectra of: (a) **PL**, (b) **M/PL**, (c) **M/PL** outgassed, (d) **PG**, (e) **M/PG**, (f) **M/PG** outgassed, (g) **M/PL/PG** and (h) **M/PL/PG** outgassed; contact time of 1 ms; only the peak regions are displayed

^{13}C NMR Chemical Shifts and Line Widths

^1H-^{13}C CP-MAS spectra of the bulk **PL** and **PG** samples, and the three polypeptide-adsorbed samples (**M/PL**, **M/PG** and **M/PL/PG**) are presented in Figure 2, with peak assignments taken from the literature.[23] The chemical shifts for the different resolved peaks along with their corresponding line widths are given in Table 2, and an example of deconvolution, for **PL** is given in Figure 3.

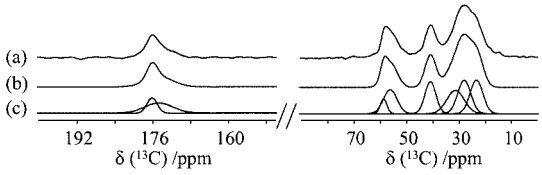

Figure 3. Deconvolution of the ^1H-^{13}C CP-MAS spectrum of **PL**: (a) experimental spectrum, (b) simulated spectrum and (c) individual components

The ^1H-^{13}C CP-MAS spectra of bulk **PL** (Figure 2, a) shows four distinct signals, which are composed of eight components (Figure 3 and Table 2): the backbone carbonyl (δ = 176.1 and 174.7 ppm), the backbone α-CH (δ = 58.3 and 55.8 ppm), the side chain ε-CH_2 (δ = 40.8 ppm), and the three remaining side chain methylene carbon atoms (δ = 31.3, 28.0 and 23.4 ppm) corresponding to the γ, β and δ-CH_2 carbon atoms, respectively. The distribution of the chemical shifts for both the carbonyl and the α-CH carbon atom clearly indicates the heterogeneous secondary structure of bulk **PL**. This is based on the well-established rule that the α-helix to β-sheet transformation in polypeptides is accompanied by a shift towards lower frequencies of the backbone α- and carbonyl carbon atoms, and a shift towards higher frequencies of the side chain β-carbon atom.[23] Intermediate shifts between these two extremes reflect the presence of random coils. For the α-CH group of **PL**, literature values of δ = 57.6 and 57.4 ppm are given for a helical conformation, and values of δ = 51.4 and 52.3 ppm for the β-sheet conformation.[23a,23c] Likewise, for the carbonyl group, literature values of δ = 175.7 and 171.5 ppm or δ = 170.4 ppm are given for the α-helix and the β-sheet, respectively.[23a] This indicates that **PL** displays a mixture of α-helical and random coil secondary structures

Table 2. ^{13}C chemical shifts (δ) and line widths (Δ) in ppm, of the different resolved peaks in the ^1H-^{13}C CP-MAS spectra; where possible, proportions of populations are indicated

	COO^-			NC=O			α-CH		ε-CH_2		γ-CH_2		β-CH_2		δ-CH_2	
	δ	Δ	%	δ	Δ	%	δ	Δ	δ	Δ	δ	Δ	δ	Δ	δ	Δ
PL			28	176.1	2.6	22	58.3	2.9	40.8	4.9	31.3	7.7	28.0	5.8	23.4	5.7
			72	174.7	6.8	78	55.8	6.1								
M/PL				173.0	5.9		54.1	4.3	40.8	2.2	30.5	6.3	27.5	2.7	23.3	5.6
PG	181.3	5.0	50	176.1	3.7	50	57.3	4.2			34.3	6.1	27.7	5.4		
			50	173.3	4.1	50	53.5	4.5								
M/PG	176.9	4.6		172.3	4.0	20	57.4	3.4			29.6	6.7	26.5	7.4		
	181.1	5.4				80	53.3	4.1								
M/PL/PG	181.0	5.8		176.5	3.2		57.4	3.4	40.7	3.0						
				173	5.9		53.3	4.1								

with proportions of about 25 and 75%, respectively (Table 2).

Similar observations can be made with regard to the **PG** ^{13}C chemical shifts (Figure 2, d). The backbone α-carbon resonance is clearly composed of two peaks at δ = 57.3 and 53.5 ppm, indicating the simultaneous α-helical and random coil secondary structures.[23a,23b] Likewise, two components are observed for the carbonyl resonance. From the deconvolutions of both the α-CH and the carbonyl resonances of **PG**, the α-helical and random coil conformations are in equal proportions (Table 2). As for **PL**, the heterogeneous nature of the **PG** secondary structure is in good agreement with the fact that the molecular weights of **PL** and **PG** are intermediate in value between low values, which favor β-sheet conformations and high values, which favor α-helices. The resonance of the carboxylic group at δ = 181.3 ppm is in the expected region for the Na salt form of the **PG** side chains.[24]

On adsorption of polylysine (sample **M/PL**, Figure 2, b), both the backbone carbonyl and α-CH peaks give rise to more symmetrical signals, shifted to lower frequencies at δ = 173.0 and 54.1 ppm, respectively. This directly reflects an overall loss of helicity of polylysine, and the adoption of a single more extended conformation. The α-helices are no longer detected. Besides, three different resolved signals are now observed for the γ, β and δ side chain methylene carbon atoms, which are shifted to lower frequencies (Table 2). This discrepancy is characterized by an apparent shielding of the three side chain −CH− carbon atoms, whereas the β-carbon peak, which should have shifted towards higher frequencies with the loss of helicity,[23a] can be directly correlated to the simultaneous approach of these carbon atoms near the negatively charged clay layer surface.[25] Furthermore, for **M/PL**, the three signals are narrower than for **PL**. The more significant narrowing occurs for the side chain ε-CH_2 peak, whose line width at half height (Δ) halves on adsorption (Table 2). This general line narrowing suggests an increase in the conformational order of these adsorbed polylysine side chain carbons within the clay interlayer space.

For **M/PG** (Figure 2, e), both the carbonyl and the α-CH peaks are shifted to lower frequencies (Table 2), indicating a similar loss of helicity. However, for the latter, a shoulder representing 20% of the signal is still observed at δ = 57.4 ppm, which indicates that the change in conformation is not complete, in contrast with **M/PL**. The side chain carboxylic peak shifts to lower frequencies, but a shoulder also remains at δ = 181.1 ppm, as in bulk **PG**. A shift to lower frequencies of the carboxylic isotropic chemical shift is in good agreement with the protonation of the side chain group.[24] Hence, on adsorption of **PG** onto **M**, most of the polyglutamic acid side chains are protonated, though a minor part remains unprotonated. Taken together with the conclusion drawn from the α-CH chemical shifts, these results confirm that **PG** side chains are directly involved in the adsorption process. However, unlike **PL** side chains, they do not have any positive charges at pH = 3.4. Therefore, to overcome the repulsion from the negative charges of the clay, carboxylic groups have to be protonated, as already shown for BSA adsorbed onto clays.[9b] Furthermore, the broadening of the $-CH_2-$ peaks (Figure 2, e) indicates that unlike for polylysine, adsorption of polyglutamic acid is not accompanied by an apparent increased ordering of the side chains.

The ^{1}H-^{13}C CP-MAS spectrum of **M/PL/PG** (Figure 2, g) displays both the characteristic ε-CH_2 signal (δ = 40.7 ppm) of **M/PL** and the characteristic carboxylic signal (δ = 181 ppm) of **M/PG**, indicating that the two polypeptides have been adsorbed. From the deconvolution of the carboxylic and carbonyl peaks and on the basis of the results of the deconvolutions on the spectra of **M/PL** and **M/PG**, an estimated ratio of 50:50 for the proportions of adsorbed **PL** and **PG** is found, which is consistent with the TG results. As for **M/PL** and **M/PG**, the carboxylic, the carbonyl and the α-CH peaks of **M/PL/PG** shift towards lower frequencies (Table 2). A part of the **PG** molecules retain the bulk secondary structure, as revealed by the carboxylic signal at δ = 181 ppm, and the α-CH signal is narrower than in bulk **PL**. Therefore, it seems that in terms of conformation, each polypeptide has been adsorbed as if the other one was not present.

When the samples were outgassed under vacuum, the ^{1}H-^{13}C CP-MAS spectra still exhibit comparable chemical shifts with those of the unheated samples (Figure 2 c, f, h), thus confirming that this high temperature treatment has not significantly modified the secondary structure of the adsorbed **PL** and **PG** molecules. This is more clearly seen for the **M/PL/PG** sample, which exhibits the highest amount of adsorbed organic matter. Only a weak modification of the conformation of some of the side chain $-CH_2-$ carbon atoms is observed, as suggested by the narrow peak at δ = 32 ppm (Figure 2, h). It must be noted that owing to the small quantities of samples left, spectra in Figure 2 c, f, h were recorded with a Bruker 2.5-mm probe, thus explaining the poor signal-to-noise ratio, particularly for **M/PG**.

X-ray Diffraction

The d_{001} peak region of each sample was recorded under controlled humidity (P/P_0 = 0.79) and after dehydration at 110 °C under vacuum (Figure 4). Unfortunately, we did not succeed in recording the diffractogram of **M/PG** after dehydration due to the lack of sample. The corresponding d_{001} values, which directly reflect the basal spacing of the samples, are presented in Table 3. This spacing is equal to the sum of the interlayer distance and the thickness of the layer, which is about 9.6 Å for a 2:1 phyllosilicate. As already reported, under a relative humidity of P/P_0 = 0.79, **M** exhibits a d_{001} value of 16.1 Å (Table 3).[12] On dehydration, the value falls to 10.5 Å, indicating the almost complete collapse of the layers, with interlayer cations partially inserted into hexagonal openings formed by the silicon tetrahedra.

Under a relative humidity of P/P_0 = 0.79, the d_{001} value of the two **PL**-containing samples (**M/PL** and **M/PL/PG**) is slightly higher (16.4 and 16.5 Å, respectively) than that

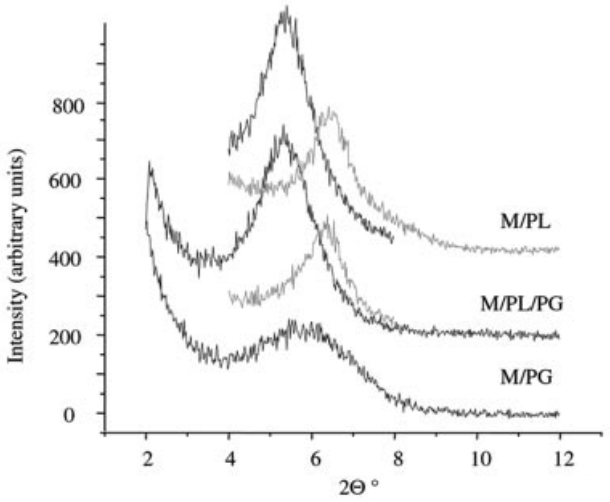

Figure 4. XRD patterns showing the d_{001} region for **M/PL** (top), **M/PL/PG** (center) and **M/PG** (bottom), under a relative humidity of 79% (black) and after dehydration (gray)

Table 3. XRD d_{001} values [Å]

	M	M/PL	M/PG	M/PL/PG
P/P_0 = 79%	16.1	16.4	15.4	16.5
Dehydrated	10.5	13.7		13.9

of **M**, whereas the d_{001} value of **M/PG** is slightly lower (15.4 Å), suggesting that the cumulative volume of adsorbed water molecules and polypeptide moieties is higher for **PL** than for **PG**. However, the highest value of 16.5 Å indicates that, in any case, only one layer of polypeptide moieties is intercalated within the interlayer space, which is consistent with the short length of the side chains of both **PL** and **PG**.[26] On dehydration, the d_{001} values for **M/PL** and **M/PL/PG** (13.7 and 13.9 Å, respectively) remain significantly higher than the thickness of the layers, and are conversely, in very good agreement with those reported for the monolayer adsorption of short chain length alkylammonium cations.[26] Therefore, only the polypeptide side chains appear to be adsorbed within the interlayer space of **M**.[11]

Nitrogen Adsorption

Nitrogen adsorption-desorption isotherms are given for samples **M** and **M/PL/PG** in Figure 5, a and are representative of the other samples. They both exhibit an important hysterisis loop, which is a mixing of type H3 and H4, characteristic of adsorbents containing slit-shaped pores.[27] The first part of these isotherms (P/P_0 between 0 and 0.2) clearly indicates a higher microporous character for **M** (type I isotherm) relative to **M/PL/PG** (type IIb isotherm), whereas the last part (P/P_0 above 0.7) reflects a higher swelling ability of **M** relative to **M/PL/PG**.

The specific surface areas calculated from the BET method are presented in Table 4, along with the corresponding proportions of microporous and external surfaces, as determined from the analyses of the *t*-plot (Figure 5, b).

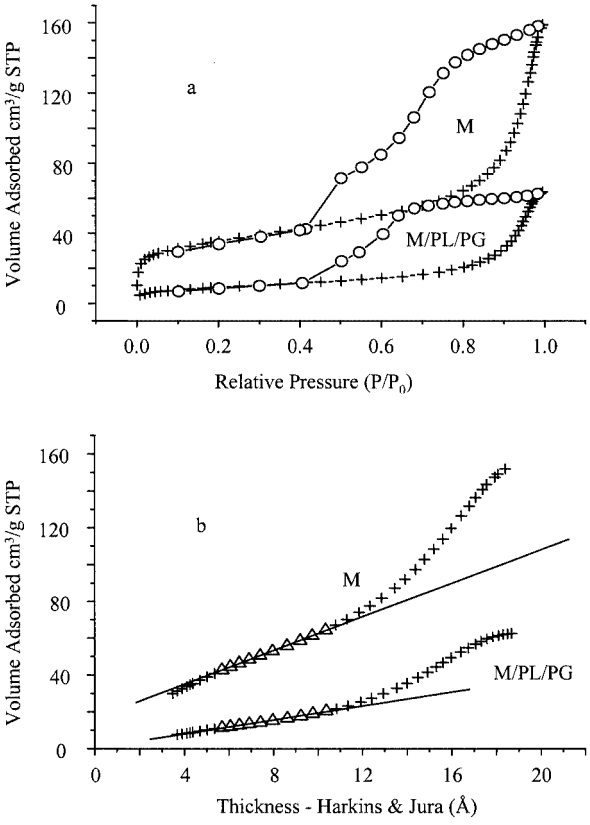

Figure 5. (a) Adsorption (+)-desorption (o) isotherms of nitrogen at 77 K on **M** and **M/PL/PG**; (b) *t*-plot representations for the same samples; triangles represent the experimental points considered for the analysis and the straight line represents the corresponding linear fit

Table 4. Specific surface areas determined from the BET measurements and proportions of external and microporous surface obtained from the *t*-plot analyses; values are expressed in m^2 per gram of dry montmorillonite and corrected for the mass of polypeptide adsorbed

	M	M/PL	M/PG	M/PL/PG
BET	128	110	92	41
External	72	63	63	37
Microporous	56	47	29	4

In the *t*-plots, the volume of nitrogen adsorbed is represented vs. the mean thickness of the adsorbed layer of nitrogen molecules,[28] and a positive intercept of the fitted linear region between ca. 5 and 10 Å directly reflects and quantifies the presence of micropores. Cumulative histogram plots (Figure 6) represent, for each sample, the sum of the microporous and external specific surface areas, which equals to the BET surface area. The above-mentioned microporosity has been attributed to the broken edge face of the particles due to the irregular stacking of the layers, which gives rise to slit-shaped pores.[29] Hence, this microporosity has been shown to be more accessible to hydration, for instance, than interlamellar porosity.[29] Therefore, although being external, this microporosity can be seen basically as interme-

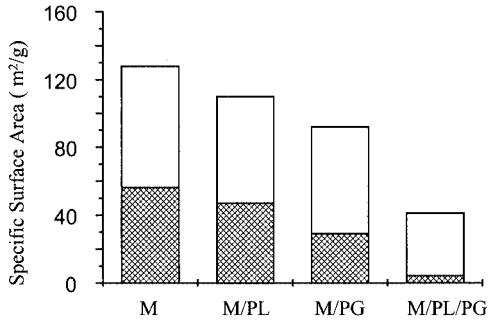

Figure 6. Cumulative histogram representing the microporous (bottom) and external (top) specific surface areas of the different samples; their sum corresponds to the BET surface for each sample

diate between the external surface of particles and the interlayer porosity.

Adsorption of polypeptides clearly leads to a decrease in the BET specific surface area of **M**, with the microporous component being the major contributor to this decrease (Figure 5, b and Figure 6). The higher BET value of **M/PL** compared with that of **M/PG** is in agreement with the thermal analyses, which have shown that on dehydration, **M/PL** has lost a more important proportion of the polypeptide than **M/PG**. In the case of **M/PL/PG**, where more polypeptides were initially adsorbed, nearly all the microporosity is lost. The external specific surface area also decreases on adsorption of the polypeptides, which indicates that the interparticle surface decreases.

Therefore, adsorption of these polypeptides can be described as a plugging process, more specifically, at the broken edges of the **M** particles, with side chains incorporated within the interlayer spaces (Scheme 2). This description agrees with all our results and explains the decrease in both the microporous character and the swelling ability of **M** on adsorption of polypeptides (Figure 5, a).

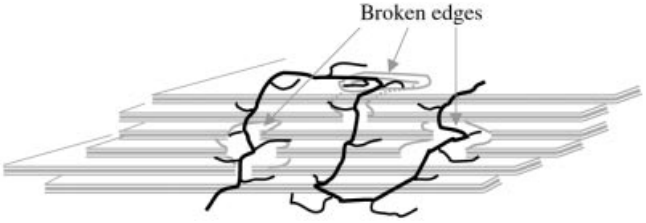

Scheme 2. Proposed description for the plugging of an unfolded polypeptide fragment at the broken edges of the **M** particles, with side chains pointing into the interlayer spaces

Conclusion

Understanding the mechanisms by which polypeptides and proteins adsorb on clay minerals is of major importance for several scientific areas, particularly in areas where this organic-inorganic interaction is at the basis of advanced composite materials. In this study, the use of complementary approaches has led to a more detailed description of the interaction between polylysine and polyglutamic acid with a synthetic montmorillonite. ^{13}C NMR chemical shifts of the backbone α- and carbonyl carbon atoms have shown that both polypeptides, which exhibit a mixture of α-helical and random coil conformations in the bulk, tend to unfold and adopt a more extended random coil structure on adsorption. Furthermore, analysis of the ^{13}C NMR line widths has shown that adsorption of the basic polylysine is accompanied by an increased ordering of the side chains, which is not the case for polyglutamic acid. However, in agreement with thermal analyses, the secondary structure of the adsorbed polypeptides is not significantly modified by heating at temperatures of up to 150 °C under vacuum. Based on this observation, we were able to compare the basal spacing of the polypeptide-adsorbed samples kept under controlled humidity ($P/P_0 = 0.79$) with that measured after dehydration under vacuum. The montmorillonite sheets collapse in the absence of adsorbed polypeptides, whereas they remain about 3.5 Å apart in their presence. Finally, nitrogen adsorption experiments, which are also based on dehydration under vacuum of the samples, were run to compare the accessible specific surface areas of the different samples. We observed that the higher the amount of polypeptide adsorbed, the lower the BET surface. The major contribution to this decrease in measured specific surface area is attributed to the microporous component of the external surface, as deduced from the analyses of the *t*-plots. All together, our results lead to the hypothesis that polypeptides are adsorbed at the periphery of the montmorillonite particles through specific interaction between the polypeptide side chains and the silicate sheets, whereas the polypeptide backbones do not enter the interlayer space.

Experimental Section

Samples: Poly-D-lysine (HBr salt) of average molecular weight 20900 and polydispersity 1.15, and poly-D-glutamic acid (sodium salt) of average molecular weight 19900 and polydispersity 1.3, were purchased from Sigma−Aldrich Chimie and used as received. Montmorillonite (**M**), whose synthesis and characterization is detailed elsewhere,[12] is a Mg-containing 2:1 dioctahedral clay with Na^+ cations in its interlayer space to balance the layer negative charge. Separate adsorption of each polypeptide was realized by mixing a solution of poly-D-lysine (**PL**) (ca. 30 mg), or poly-D-glutamic acid (**PG**) (ca. 30 mg), dissolved in a 15-mL acidic solution (pH = 3.4) with a solution of montmorillonite (**M**) (500 mg), initially suspended for 5 d in 25 mL of the same acidic buffer, at 10 °C for 6 h. Co-adsorption of the two polypeptides was realized under similar conditions by adding a solution of **PL** (50 mg) and **PG** (50 mg) dissolved in 50 mL of the acidic buffer to a solution of **M** (240 mg), initially suspended in 25 mL of the acidic buffer. After filtration through 0.45 μm filters and repeated washes with the buffer and deionized water, the three polypeptide-adsorbed samples **M/PL**, **M/PG** and **M/PL/PG** were dried overnight at room temperature in air and stored at 4 °C.

Thermal Analysis: TG-DTA measurements were carried out with a Setaram Labsys apparatus under air-flow condition, with a heating rate of 5 °C/min, from 18 to 750 or 800 °C.

X-ray Powder Diffraction: X-ray diffractograms were recorded with a STOE STADI-P powder X-ray diffractometer, equipped with a linear position-sensitive detector ($2\theta = 6°$) in Debye−Scherrer geometry and employing Ge-monochromated Cu-$K_{\alpha 1}$ radiation (λ = 1.5406 Å). Records, in the range $2\theta = 2-12°$, were performed on samples under controlled humidity ($P/P_0 = 0.79$) and on samples dehydrated at 110 °C under vacuum for 10 h. For the former, capillaries were filled with powder kept under controlled humidity, just before starting the experiment, whereas for the latter, capillaries were filled in a glove box under argon. In both cases, the capillaries were sealed immediately after filling up.

N_2 Adsorption: Complete nitrogen gas adsorption-desorption cycles were obtained with a Micromeritics ASAP 2001 apparatus. BET specific surface areas were determined from the initial part of the adsorption branches (typically in the range $P/P_0 = 0.04-0.2$), and the *t*-plot analysis of the adsorption permitted the determination of the microporous and external surface proportions. Prior to experiments, about 100 mg of each sample was outgassed to a residual pressure of less than 0.8 Pa at 110 or 150 °C for about 15 h.

Solid-State NMR Spectroscopy: ^{13}C NMR spectroscopic experiments were run with a Bruker DSX 400 spectrometer operating at frequencies of 100.6 MHz, and a Bruker MSL 300 spectrometer operating at a frequency of 75.4 MHz. ^1H-^{13}C Cross-Polarization-MAS (CP-MAS) experiments were performed using a Bruker double-channel 4-mm probe or a Bruker double-channel 2.5-mm probe. Hartmann−Hahn matching for the ^1H-^{13}C CP-MAS experiments was set on adamantane for ^1H and ^{13}C radio-frequency fields of ca. 60 kHz. Proton T_1 spin-lattice relaxation times ranged between 100 and 500 ms for the different proton species observed in the ^1H MAS spectra of mineral/polypeptide products. In the case of bulk polypeptides, rotors were packed in a glove box under argon in order to prevent interaction with ambient moisture. This resulted in higher ^1H T_1 values (ca. 1 s), mainly attributed to the absence of the paramagnetic O_2 relaxing agent. Chemical shifts for ^{13}C spectra were referenced to adamantane (δ_C = 29.47 ppm for the low-frequency peak). Deconvolution of the ^1H-^{13}C CP-MAS spectra was performed with the WINFIT software.[30]

Acknowledgments

We are grateful to the Region Champagne − Ardennes for financial support through the grant of R. D. G. Drs. L. Delmotte and X. Bourdon are acknowledged for helpful discussions.

[1] H. Quiquampoix, *Mechanisms of protein adsorption on surfaces and consequences for extracellular enzyme activity in soil*, in Soil Biochemistry (Eds: J. M. Bollag, G. Stotzky), Marcel Dekker, Inc., New York, **2000**, vol. 10, p. 171−206.
[2] C. Causserand, K. Jover, P. Aimar, M. Meireles, *J. Membr. Sci.* **1997**, *137*, 31−44.
[3] E. P. Giannelis, *Adv. Mater.* **1996**, *8*, 29−35.
[4] [4a] A. Clearfield, *Chem. Mater.* **1998**, *10*, 2801−2810. [4b] C. Breen, R. Watson, *J. Colloid Interface Sci.* **1998**, *208*, 422−429.
[5] M. R. Sarmento, J. G. Oliveira, R. B. Boulton, *Int. J. Food. Sci. Tech.* **2000**, *35*, 41−47.
[6] J. T. Kloprogge, S. Komarneni, J. E. Amonette, *Clays Clay Miner.* **1999**, *47*, 529−554.
[7] [7a] W. Norde, *Adv. Colloid Interface Sci.* **1986**, *25*, 267−328. [7b] C. A. Haines, W. Norde, *Colloids Surf. B* **1994**, *2*, 517−525. [7c] S. Staunton, H. Quiquampoix, *J. Colloid Interface Sci.* **1994**, *166*, 89−94. [7d] A. Pantazaki, M. H. Baron, M. Revault, C. Vidal-Madjar, *J. Colloid Interface Sci.* **1998**, *207*, 324.
[8] [8a] R. K. Sandwick, K. J. Schray, *J. Colloid Interface Sci.* **1987**, *115*, 130. [8b] H. Quiquampoix, S. Staunton, M. H. Baron, R. G. Ratcliffe, *Colloids Surf. A* **1993**, *75*, 85−93.
[9] [9a] M. H. Baron, M. Revault, S. Servagent-Noinville, J. Abadie, H. Quiquampoix, *J. Colloid Interface Sci.* **1999**, *214*, 319−332. [9b] S. Servagent-Noinville, M. Revault, H. Quiquampoix, M. H. Baron, *J. Colloid Interface Sci.* **2000**, *221*, 273−283.
[10] C. H. Yu, M. A. Norman, S. Q. Newton, D. M. Miller, B. J. Teppen, L. Schäfer, *J. Mol. Struct.* **2000**, *556*, 95−103.
[11] [11a] R. D. Gougeon, M. Reinholdt, L. Delmotte, J. Miehé-Brendlé, J-M. Chézeau, R. Le Dred, R. Marchal, P. Jeandet, *Langmuir* **2002**, *18*, 3396−3398. [11b] T. Coradin, O. Durupthy, J. Livage, *Langmuir* **2002**, *18*, 2331−2336. [11c] J. N. Cha, G. D. Stucky, D. E. Morse, T. J. Deming, *Nature* **2000**, *403*, 289−292.
[12] M. Reinholdt, J. Miehé-Brendlé, L. Delmotte, M-H. Tuilier, R. Le Dred, R. Cortès, A-M. Flank, *Eur. J. Inorg. Chem.* **2001**, 2831−2841.
[13] V. L. Fernandez, J. A. Reimer, M. M. Denn, *J. Am. Chem. Soc.* **1992**, *114*, 9634−9642.
[14] W. Xie, Z. Gao, K. Liu, W-P. Pang, R. Vaia, D. Hunter, A. Singh, *Thermochim. Acta* **2001**, *339*, 367−368.
[15] W. J. Shaw, J. R. Long, J. L. Dindot, A. A. Campbell, P. S. Stayton, G. P. Drobny, *J. Am. Chem. Soc.* **2000**, *122*, 1709−1716.
[16] [16a] A. Golchin, P. Clarke, J. M. Oades, *Biogeochemistry* **1996**, *34*, 71−97. [16b] D. W. Hopkins, J. A. Chudek, S. F. I. Haslam, E. A. Webster, *NMR Microbiol.* **2000**, 431−451. [16c] N. J. Mathers, X. A. Mao, Z. H. Xu, P. G. Saffigna, S. J. Berners-Price, M. C. S. Perera, *Aust. J. Soil Res.* **2000**, *38*, 769−787.
[17] H. Quiquampoix, R. G. Ratcliffe, *J. Colloid Interface Sci.* **1992**, *148*, 343−352.
[18] E. S. Boeck, P. V. Coveney, N. T. Skipper, *J. Am. Chem. Soc.* **1995**, *117*, 12608−12617.
[19] O. Sieskind, *C. R. Acad. Sci. Fr.* **1960**, *250*, 2392−2393.
[20] G. Lagaly, *Clay Minerals* **1981**, *16*, 1−21.
[21] R. Greene-Kelly, *Clay Min. Bull.* **1964**, *5*, 392−400.
[22] P. T. Hang, G. W. Brindley, *Clays Clay Miner.* **1970**, *18*, 203−212.
[23] [23a] H. R. Kricheldorf, D. Müller, *Macromolecules* **1983**, *16*, 615−623. [23b] A. Shoji, O. Takuo, H. Saitô, R. Tabeta, I. Ando, *Macromolecules* **1984**, *17*, 1472−1479. [23c] H. Saitô, *Magn. Reson. Chem.* **1986**, *24*, 835−852.
[24] Z. Gu, A. McDermott, *J. Am. Chem. Soc.* **1993**, *115*, 4282−4285.
[25] C. H. Chiang, N. I. Liu, J. L. Koenig, *J. Colloid Interface Sci.* **1982**, *86*, 26−34.
[26] A. R. Mermut, G. Lagaly, *Clays Clay Miner.* **2001**, *49*, 393−397.
[27] F. Rouquerol, J. Rouquerol, K. Sing, *Adsorption by Powders & Porous Solids*, Academic Press, San Diego, **1999**.
[28] J. H. de Boer, B. C. Lippens, B. G. Linsen, J. C. P. Broekhollf, A. Van der Heuvel, Th. J. Osinga, *J. Colloid Interface Sci.* **1966**, *21*, 405.
[29] J. M. Cases, I. Bérend, G. Besson, M. François, J. P. Uriot, F. Thomas, J. E. Poirier, *Langmuir* **1992**, *8*, 2730−2739.
[30] D. Massiot, Web site: http://crmht.cnrs-orleans.fr/Pole1/ThemeDM/

Received July 24, 2002
[I02416]